Full Length Article

First-principles study of oxygen-related defects on 4H-SiC surface: The effects of surface amorphous structure

Yu-ichiro Matsushita[a,*], Yoritaka Furukawa[a], Yasuto Hijikata[b], Takeshi Ohshima[c]

[a] Department of Applied Physics, The University of Tokyo, Tokyo 113-8656, Japan
[b] Graduate School of Science and Engineering, Saitama University, Saitama 338-8570, Japan
[c] National Institutes for Quantum and Radiological Science and Technology (QST), Takasaki, Gunma 370-1292, Japan

A B S T R A C T

We report our first-principles calculations that clarify the electronic states of oxygen-related defects in the 4H-SiC bulk and on the 4H-SiC surface and how they are affected by the surface amorphous structure due to oxidation. It is experimentally reported that thermally oxidized 4H-SiC contains an abundant amount of single-photon sources on its surface (surface SPSs) and that their emitting wavelengths have variance. However, the microscopic mechanism is not clarified yet. In our work, we demonstrate that the energy levels of the oxygen-related defects on the surface are altered sensitively by the local atomic structure of the amorphous surface leading to variations in the wavelengths.

Single-photon sources (SPSs) are an essential element for quantum information processing and quantum computing technology. When an electron pumped up to an excited state by light goes back to the ground state, the SPS generates a single photon with a wavelength corresponding to the HOMO(highest-occupied-molecular orbital)-LUMO (lowest-unoccupied-molecular orbital) gap. For practical application of SPS devices, solid devices are desirable because of its stability and mobility. Some defect structures in many semiconductor materials are known to date to work as SPSs such as NV^- center in diamond and Zn vacancy (V_{Zn}) in ZnO crystal [1]. Recently, SiC is getting much attention for SPS devices, since SiC contains various types of intrinsic defects that behave as an SPS. Many of SPSs in SiC bulk are already identified, such as silicon vacancy (V_{Si}) [2,3], carbon-silicon di-vacancy ($V_C V_{Si}$) [4], and antisite-vacancy pair ($C_{Si} V_C$) [5]. In addition, it is reported that the brightness of SPSs in SiC can be controlled electrically by embedding the SPSs in SiC-MOS (metal-oxide semiconductor) devices. This opens a possibility of new optoelectronic devices [6–9].

Interestingly, a large number of bright SPSs have been reported to emerge on the surface (surface SPSs) of SiC through thermal oxidation on Si-[7,10,11] and C-face[8,10] both. These SPSs have different characters from other known SPSs. One interesting point is that the surface SPSs are more than twice as bright as even NV^- center in diamond [7]. Another striking feature is that there is a certain amount of variance in their emitting wavelengths of the zero-phonon line (ZPL) [8,11]. However, the microscopic mechanisms of the variance in the ZPL are not clarified yet. One possible scenario is an interplay between an SPS and a stacking fault[7]: The wave function of the excited state around a surface SPS is modulated by the stacking fault depending on the SPS position in real space. The stacking fault structure in SiC surface is reported both experimentally[12,13] and theoretically[14] and such interaction between a surface SPS and a stacking fault is likely. However, it is reported that there is no clear relation observed between the SPS position near the single Schottky-stacking fault (SSSF) and its ZPL [15]. Only brightness is affected by the SSSF. This fact might show that the wide variety of ZPL of surface SPSs cannot be explained by the stacking fault alone. Microscopic understanding of the variances in the ZPL of the surface SPSs is yet to be achieved.

In this work, we propose another possible mechanism to explain the variances in the ZPL of surface SPSs on the basis of the density-functional theory (DFT)[16] with the Kohn-Sham scheme [17]. The surface of a thermally oxidized SiC is thought to be amorphous through chemical absorption of O atoms, forming complex atomistic structures. Therefore, the different local atomic structures near a surface SPS can cause changes in the ZPL of the surface SPS in the similar way to a defect level in amorphous SiO_2[18,19]. The thermal process is conceivable to introduce many O-related defects (O-defects) on the surface having a possibility of behaving as SPSs. Furthermore, a recent experiment done by us points out that the surface SPSs incorporate O atoms by using the oxygen isotope [20]. Therefore, we focus on O-defects on the surface of 4H-SiC in this work. Also, we have investigated
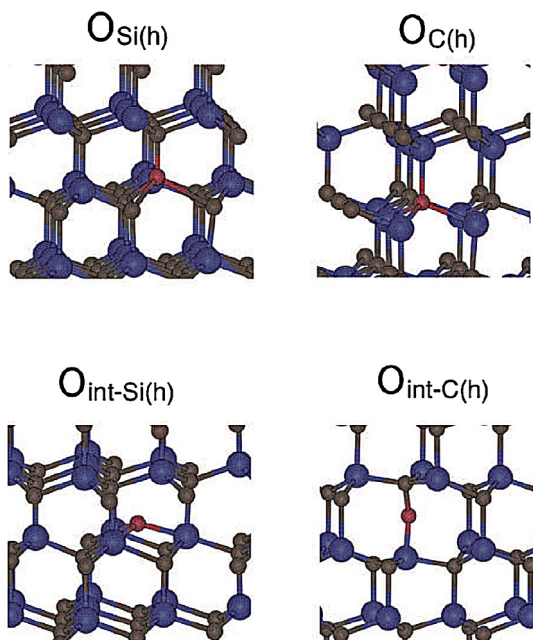
Fig. 1. Optimized O-defects in 4H-SiC bulk Viewed from the [1 1 $\bar{2}$ 0] direction. Blue (brown) balls depict Si (C) atoms, and red ones depict O atoms. (For interpretation of the references to colour in this figure legend, the reader is referred to the web version of this article.)
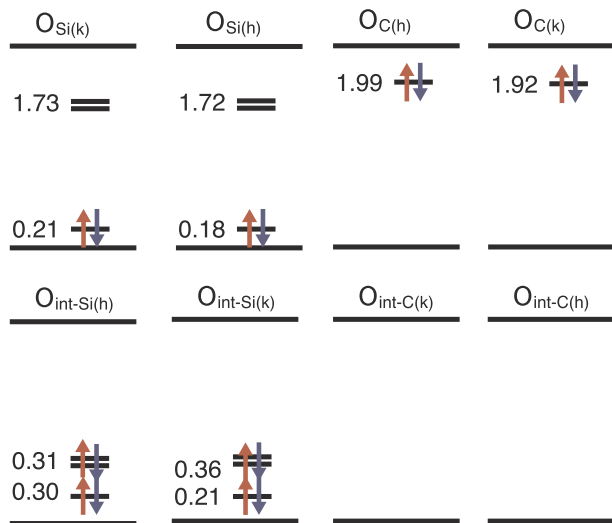
Fig. 2. Calculated mid-gap levels of various types of O-defects in 4H-SiC bulk. The top (bottom) line indicates the valence-band maximum (VBM) (conduction-band minimum (CBM)) of the 4H-SiC bulk. Differences from VBM energies are shown in eV. Red upward (blue downward) arrows indicate the occupation of the majority- (minority-) spins. (For interpretation of the references to colour in this figure legend, the reader is referred to the web version of this article.)

the effects of distortion on the variances of the ZPL. It is because the distortion in SiC/SiO$_2$ interfaces is observed in experiments[21,22] and is also a conceivable factor to affect the ZPL of the surface SPSs.

All calculations, including both the structural optimizations and the static electronic-structure calculations, have been performed by Vienna *ab initio* Simulation Package (VASP) with PAW method [23,24] using PBE exchange-correlation functional [25] in the generalized gradient approximation (GGA). Note that while the GGA underestimates band gaps by about 50%, the amount of energy-level shifts can be evaluated quantitatively. In fact, thought the calculated band gap of 4H-SiC is underestimated to 2.4 eV in comparison to experimental value 3.3 eV,
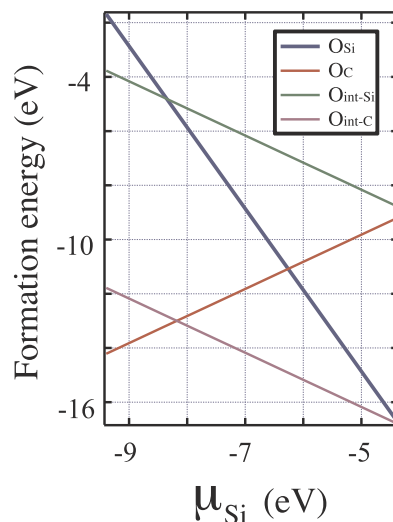
Fig. 3. Calculated formation energies of various types of O-defects in the 4H-SiC bulk.
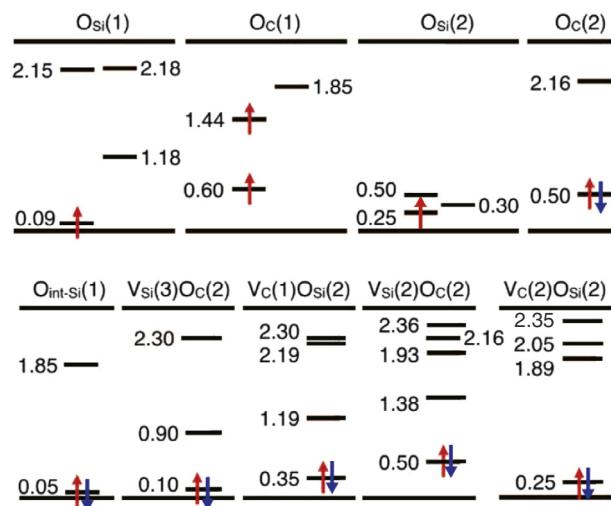
Fig. 4. Calculated mid-gap levels of various types of O-defects in the 4H-SiC oxidized surface. The top (bottom) line indicates the valence-band maximum (VBM) (conduction-band minimum (CBM)) of the 4H-SiC bulk. Differences from VBM energies are shown in eV. Red upward (blue downward) arrows indicate the occupation of the majority- (minority-) spins. (For interpretation of the references to colour in this figure legend, the reader is referred to the web version of this article.)
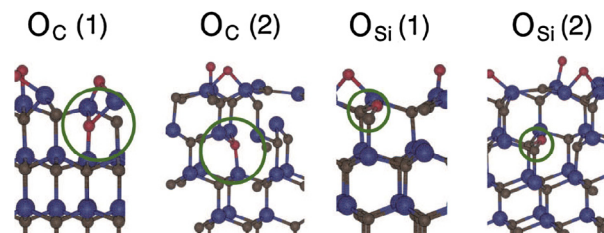
Fig. 5. Optimized O-defects on 4H-SiC surface viewed from the [1 $\bar{1}$ 0 0] direction (a) and from the [1 1 $\bar{2}$ 0] direction (b) (c) (d). Blue (brown) balls depict Si (C) atoms, and red ones depict O atoms. Green circles point out the substituting O atoms. (For interpretation of the references to colour in this figure legend, the reader is referred to the web version of this article.)
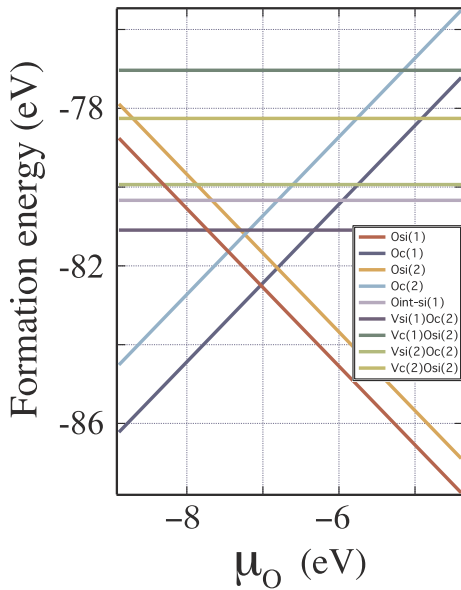
Fig. 6. Calculated formation energies of various types of O-defects in the 4H-SiC surface.
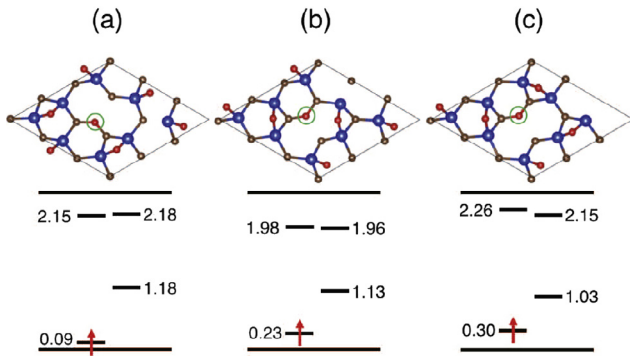
Fig. 7. Surface structures of 4H-SiC with several different oxidation patterns and the corresponding mid-gap levels. $O_{Si}(1)$ defects are indicated by green circles. Atoms in the second and deeper bilayers are omitted. Energies are shown in the unit of eV. The top (bottom) line of each diagram indicates the VBM (CBM) of the 4H-SiC bulk. Black lines on the left (right) stand for majority (minority) spins, where occupied levels are indicated by red upward (blue downward) arrows. (For interpretation of the references to colour in this figure legend, the reader is referred to the web version of this article.)
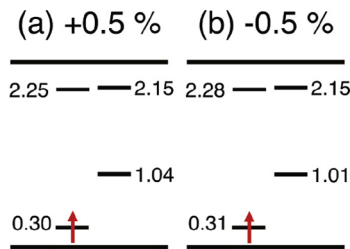
Fig. 8. Calculated mig-gap levels of $O_{Si}(1)$ defect with (a) +0.5% strain and (b) −0.5% in-plane strain. The surface configurations of both (a) and (b) are same as that of Fig. 7 (c), with small displacements after structural optimizations.

the calculated band-gap variations among SiC polytypes are well reproduced[26]. We adopted a slab model with 5 bilayer thickness to simulate the amorphous surface structure of Si-face. By using the slab model, the calculated energy gap of the slab is usually larger than that of bulk due to the quantum confinement effect. However, the 5-bilayer slab thickness of SiC used in present work is enough large exhibiting the

band gap of 2.4 eV the same as that of SiC bulk. The other side (C-face) of the slab surface with one-bilayer thickness is fixed at the crystallographic position and terminated by H atoms. The thickness of the vacuum layer has been set to 9 Å, which is large enough to ignore the interactions between the adjacent slabs. The surface stacking sequence is set to ABC because such ABC-stacking surface structure is known to be stable than the BCBA-stacking surface structure[14]. The convergence criterion of force is set to be 0.01 eV/Å. We consider a 3×3 supercell model of 4H-SiC in lateral plane. Γ-centered Monkhorst-Pack $2 \times 2 \times 1$ k-point sampling and the cutoff energy 450 eV have been applied to every calculation, assuring the convergence of the total energy within 0.1 eV.

Before the investigation of O-defects on surface, we first calculated the O-defects embedded in 4H-SiC bulk. We have checked the electronic energy levels of three different kinds of O-defects: Oxygen substitution at C site (O_C), oxygen substitution at Si site (O_{Si}), and interstitial oxygen (O_{int}). By considering that the two inequivalent sites exist in the bulk, i.e., so-called k (cubic) and h (hexagonal) sites, we distinguish each site with a label, (k) or (h). Regarding the interstitial sites, we use labels such as O_{int-Si} and O_{int-C} in the sense of an interstitial site located at a backbond of a Si and C atom, respectively. We prepared $3 \times 3 \times 2$ supercells including a defect and optimized the structures.

The yielded defect structures, electronic levels, and formation energies are shown in Figs. 1, 2, and 3, respectively. The defect levels plotted in Fig. 2 are extracted from the Γ point of the calculations. The formation energy as a function of μ_O plotted in Fig. 3 is defined as

$$F = E^{\text{total}} - \mu_{Si}N_{Si} - \mu_C N_C - \mu_O N_O, \qquad (1)$$

where μ_{Si}, μ_C, and μ_O are the chemical potential of Si, C, and O, respectively. N_{Si}, N_C, and N_O are the number of Si, C, and O atoms in the simulation cell, respectively. These chemical potentials are determined as follows:

$$\mu_C = E_{SiC} - \mu_{Si} \qquad (2)$$

and

$$\mu_{Si} = E_{SiO_2} - 2\mu_O, \qquad (3)$$

where E_{SiC} and E_{SiO_2} are the calculated total energy of bulk SiC and of SiO_2 at 0 K. The range of the μ_O is −4 eV (O-rich condition corresponding to the O_2 molecule) to −10 eV (O-poor condition corresponding to SiO_2).

We have found that the O_{int-C} defect is unstable and the O atom prefers to go into the network of SiC to form a Si−O−C bond as shown in Fig. 1. Consequently, there are no electronic levels in SiC energy gap region as shown in Fig. 2. In contrast, the other defect structures are stable and the O atom of all the other defects locates at each C_{3v}(point group)-symmetry position. In $O_{Si(h)}$ and $O_{C(h)}$ defects, O atoms occupy the 4-fold-coordinate position: the bond length of one O−C (O-Si) is 1.48 (1.89)Å and those of the other three are 2.21 (2.04)Å. The O atom in the $O_{int-Si(h)}$ takes 3-fold coordination. We have found that the O-defects, O_{Si}, O_C, and O_{int}, generate mid-gap states in SiC energy gap. Importantly, we cannot see big differences between two inequivalent sites, h and k sites, in any defect types. In fact, the variation of the energy levels of the mid-gap states is within 0.09 eV. These results are attributed to the structural similarity between them.

The effect of the structural similarity can also be seen in the formation energies. We cannot see big differences in formation energy between h and k sites, less than 0.25 eV: $O_{Si(h)}$ is lower in energy than $O_{Si(k)}$ by 0.01 eV, $O_{C(k)}$ is lower than the other by 0.21 eV, $O_{int-Si(k)}$ is lower than the other by 0.13 eV, and Si(k)-O-C(k), a yielded structure after the structural optimization from $O_{int-C(h)}$, is lower than Si(h)-O-C(h), a yielded structure after the structural optimization from $O_{int-C(k)}$ by 0.14 eV. Comparison among the stabler defects of each kind is done in Fig. 3. As clearly seen from the figure, in the O-rich region (−8 ⩽ μ_O ⩽ −4 eV), the O_{int-C} defect is the most likely and the O_{Si} defect follows. In contrast, the O_C defect is stabler in the O-poor region

$(-10 \leqslant \mu_O \leqslant -8$ eV). The O_{int-Si} defect seems unlikely because of the high formation energy.

Next, to prepare an oxidized Si-face, we have initially placed O atoms near the surface and relaxed the structure to obtain a stable atomic configuration, annihilating all the dangling bonds of Si atoms. In actual experiments for the surface SPSs, oxidization is done under relatively low temperature and short oxidation conditions. With such oxidation situations, 30 min. at 800 °C, just 1–2 bilayers are thought to be oxidized. Our calculation models mimic such an oxidized surface. We introduced various types of O-defects to the oxidized surface and investigated the electronic states. Numerous types of O-defects are conceivable on the surface: Vacancies, substitution, interstitials, and their combinations. In particular, we have calculated the following O-defects, O_{Si}, O_C, $O_{Si}V_C$, O_CV_{Si}, O_CC_{Si}, O_{int-Si}, and O_{int-C}. We put these defects in either first or second bilayer counted from the surface. The layer position of the defects is indicated by a number in parentheses such as $O_{Si}(1)$ or $O_{Si}(2)$. As shown in Fig. 4, many of the defects form mid-gap states. In particular, it is clearly seen that O_{Si} and O_C defects on the surface generate different energy levels from those in bulk shown in Fig. 2. It is because their defect structures are quite different: In bulk, the O atoms take 4-fold coordination for both O_{Si} and O_C, while the O atoms on the surface prefer 2-fold coordination for O_{Si} and 3-fold co-ordination for O_C as shown in Fig. 5. These structural differences cause different energy levels. Another noteworthy point in the results is that even if the same kind of defect it is, their mid-gap states strongly depend on the defect position in contrast to the SPSs in bulk, i.e., $O_C(1)$ and $O_C(2)$ give quite different energy levels. It is also found that $O_{Si(1)}$, $O_{C(1)}$, and $O_{Si(2)}$ defects have spin structure. The observation of the spin structure can be a finger print of the defects.

Another notable thing is the formation energy of them. Fig. 6 shows the comparison among the calculated formation energies of the defects as a function of μ_O. We have found that in O-rich region ranging from -7 to -4 eV, O_{Si} defects are stabilized while in O-poor region O_C defects are likely. Therefore, from this result O_{Si} defects are likely near the surface or interfaces with SiO_2.

Furthermore, we focus on $O_{Si}(1)$ defects embedded in amorphous surface and investigated how the amorphous structure on the surface affects its mid-gap levels. We made three samples including an $O_{Si}(1)$ defect as shown in Fig. 7. As clearly seen in the figure, the different local atomic structure leads to different HOMO-LUMO gap ranging from 1.73 eV to 2.06 eV. The energy difference is 0.33 eV. This result manifests the HOMO-LUMO gap can vary depending on the local atomic structures near the defect by at least 0.3 eV. Experimentally observed energy variance in the ZPL is also the order of 0.35 eV [11]. Thus, we have found that the different local atomic structure on the amorphous surface can explain the experimentally obtained variances in the ZPL. In addition, the total energy differences among them are within 0.5 eV, derived from the distortion energy of different local structure of SiO_2.

We have also investigated the distortion effect on electronic states as well by applying distortion to the O_{Si} defect in lateral direction. The applied amount of distortion is -0.5% and 0.5%, of the experimentally observed extent[21]. The results are shown in Fig. 8. We have found that the mid-gap states do not change so much: The variation is only 0.02 eV, much smaller than the experimentally observed variations. These results clearly manifest that the distortion is difficult to explain the ZPL variation in experiments.

In conclusion, we report our first-principles calculations based on the density-functional theory that clarify the electronic states of oxygen-related defects (O-defects) in the 4H-SiC bulk and on the 4H-SiC surface and how they are affected by the surface amorphous structure

due to the oxidation. It is experimentally reported that thermally oxidized 4H-SiC contains an abundant amount of single-photon sources on its surface (surface SPSs) and that their emitting wavelengths have about 0.3 eV variance. Such large variance of the emitting wavelengths is one curious feature peculiar to the surface SPSs. However, the microscopic mechanism is not clarified yet. In this work, we focused on O-defects, one of plausible surface SPS defects on the oxidized surface SiC, and showed that the energy levels of the mid-gap states are altered sensitively by the local atomic structure of the amorphous surface by ~ 0.3 eV. We have also discussed that the effect of the in-plane strain of the SiC surface on the electronic levels is too small to explain the experimentally observed ZPL variation. Our findings imply that oxygen-related surface SPSs have a wide range of variety both in the defect types and the emitting wavelengths.

References

[1] A.J. Morfa, B.C. Gibson, M. Karg, T.J. Karle, Andrew D. Greentree, P. Mulvaney, S. Tomljenovic-Hanic, Nano Lett. 12 (2012) 949.
[2] M. Widmann, S.-Y. Lee, T. Rendler, N.T. Son, H. Fedder, S. Paik, L.-P. Yang, N. Zhao, S. Yang, I. Booker, A. Denisenko, M. Jamali, S.A. Momenzadeh, I. Gerhardt, T. Ohshima, A. Gali, E. Janzén, J. Wrachtrup, Nat. Mater. 14 (2015) 164.
[3] T. Ohshima, T. Satoh, H. Kraus, G.V. Astakhov, V. Dyakonov, P.G. Baranov, J. Phys. D: Appl. Phys. 51 (2018) 333002.
[4] D.J. Christle, A.L. Falk, P. Andrich, P.V. Klimov, J.U. Hassan, N.T. Son, E. Janzén, T. Ohshima, D.D. Awschalom, Nat. Mater. 14 (2015) 151.
[5] S. Castelletto, B.C. Johnson, V. Ivády, N. Stavrias, T. Umeda, A. Gali, T. Ohshima, Nat. Mater. 13 (2014) 151.
[6] A. Politi, J.C.F. Matthews, J.L. O'Brien, Science 325 (2009) 1221.
[7] A. Lohrmann, N. Iwamoto, Z. Bodrog, S. Castelletto, T. Ohshima, T.J. Karle, A. Gali, S. Prawer, J.C. McCallum, B.C. Johnson, Nat. Commun. 7 (2015) 7783.
[8] Y. Abe, T. Umeda, M. Okamoto, R. Kosugi, S. Harada, M. Haruyama, W. Kada, O. Hanaizumi, S. Onoda, T. Ohshima, Appl. Phys. Lett. 112 (2018) 031105.
[9] C.F. de las Casas, D.J. Christle, J. Ul Hassan, T. Ohshima, N.T. Son, D.D. Awschalom, Appl. Phys. Lett. 111 (2017) 262403.
[10] A. Lohrmann, S. Castelletto, J.R. Klein, T. Ohshima, M. Bosi, M. Negri, D.W.M. Lau, B.C. Gibson, S. Prawer, J.C. McCallum, B.C. Johnson, Appl. Phys. Lett. 108 (2016) 021107.
[11] H. Tsunemi, T. Honda, T. Makino, S. Onoda, S.-I. Sato, Y. Hijikata, T. Ohshima, Mater. Sci. Forum 924 (2018) 204.
[12] U. Starke, J. Schardt, J. Bernhardt, M. Franke, K. Heinz, Phys. Rev. Lett. 82 (1999) 2107.
[13] J.B. Hannon, R.M. Tromp, N.V. Medhekar, V.B. Shenoy, Phys. Rev. Lett. 103 (2009) 256101.
[14] Y.-i. Matsushita, A. Oshiyama, Nano Lett. 17 (2017) 6458.
[15] Y. Hijikata, private communication.
[16] P. Hohenberg, W. Kohn, Phys. Rev. B 136 (1964) 864.
[17] W. Kohn, L.J. Sham, Phys. Rev. A 140 (1965) 1133.
[18] P.V. Sushko, S. Mukhopadhyay, S.S. Mysovsky, V.B. Sulimov, A. Taga, A.L. Shluger, J. Phys.: Condens. Matter 17 (2005) S2115.
[19] T. Kaneko, N. Tajima, T. Yamasaki, J. Nara, T. Schimizu, T. Kato, T. Ohno, App. Phys. Express 11 (2018) 011302.
[20] Y. Hijikata, T. Horii, Y. Furukawa, Y.-i. Matsushita, T. Ohshima, in preparation, 2018.
[21] A.D. Hatmanto, K. Kita, Appl. Phys. Express 11 (2018) 011201.
[22] X. Li, A. Ermakov, V. Amarasinghe, E. Garfunkel, T. Gustafsson, L.C. Feldman, Appl. Phys. Lett. 110 (2017) 141604.
[23] G. Kresse, J. Furthmüller, Phys. Rev. B 54 (1996) 11169.
[24] G. Kresse, D. Joubert, Phys. Rev. B 59 (1999) 1758.
[25] J.P. Perdew, M. Ernzerhof, K. Burke, J. Chem. Phys. 105 (1996) 9982.
[26] Y.-i. Matsushita, Atsushi Oshiyama, Phys. Rev. Lett. 112 (2014) 136403.